A Flexible PET-based Wearable Sensor for Arterial Pulse Waveform Measurement

Dan Wang[1], Dean Krusienski[2] and Zhili Hao[1]
[1]*Department of Mechanical and Aerospace Engineering, Old Dominion University, Norfolk, VA, U.S.A.*
[2]*Electrical and Computer Engineering, Old Dominion University, Norfolk, VA, U.S.A.*

Keywords: Wearable Sensors, Microfluidics, Arterial Pulse Waveform, Baseline Drift, Health Monitoring.

Abstract: In light of the need of health monitoring, the paper presents a flexible polyethylene terephthalate (PET)-based wearable sensor for arterial pulse waveform measurement. The sensor encompasses a polydimethylsiloxane (PDMS) microstructure embedded with an electrolyte-enabled 5×1 transducer array, which spans 6mm and has a spatial resolution of 1.5mm. A pulse signal exerts a deflection on the microstructure and is recorded as a resistance change by a transducer at the site of the pulse. An untrained individual can easily align the sensor on a targeted artery with a negligible margin and then acquire the arterial pulse waveform continuously and non-invasively. This sensor is fabricated using microfluidics technology and thus features low cost for mass production. The sensor is hand-held on an artery and records its pulse signal for a 10s period, which bears baseline drift, due to the respiration and the motion artifact. Discrete Meyer Wavelet Transform (DMWT) and Cubic Spline Estimation (CSE) are employed to remove baseline drift in a pulse signal. The pulse waveform is expressed in terms of the sensor deflection as a function of time. Carotid arterial pulse waveforms are measured by the sensor on three subjects at rest and on two subjects post-exercise. Additionally, radial arterial waveforms are measured on one subject at rest. The measured pulse pattern change of the two subjects between at rest and post-exercise is consistent with the literature. As the pulse transmits from central (carotid) to peripheral (radial) for one subject, the ratio of amplitude of main peak to amplitude of dicrotic wave goes up and the up-stroke time becomes shorter. This is consistent with the related observations in the literature. Thus, the limited amount of data collected here demonstrates the feasibility of using the sensor as a wearable health monitoring device.

1 INTRODUCTION

Arterial pulse waveforms are intimately associated with the physiological conditions of the cardiovascular system and thus provide valuable information of the diagnosis and treatment of Cardiovascular disease (CVD) (Lin et al., 2013). As reported by the World Health Organization, CVDs are the number one cause of death globally: more people die annually from CVDs than from any other cause (Lin et al., 2013). For this reason, various devices and techniques have been developed for arterial pulse waveform measurement, or arterial tonometry. To date, a few devices for arterial tonometry, including a flexible pulse monitoring system from Pressure Profile System (PPS) (Hu et al., 2012) and CASPal system that measures Central Aortic Systolic Pressure (CASP) from HealthStats (Saugel et al., 2014), are commercially available and have been successfully employed for arterial pulse waveform measurement. However, current tonometric devices are unsuitable for not only wearing with relative comfort but also for an untrained individual to use at home.

Recently, based on microfluidics technology, a polyethylene terephthalate (PET)-based sensor array to monitor arterial pressure waveforms is developed (Digiglio et al., 2014). Although this PET-based sensor array offers quite a few attractive features for daily use by an untrained individual, it entails complex fabrication process, including bonding three layers together and injecting electrolyte into each individual sensor in the sensor array. Meanwhile, its spatial resolution of 5mm×5mm is well above the typical size of a carotid and radial artery, and thus the sensor array may risk having no transducers placed right above the target artery.

To address the above-mentioned two issues

Wang, D., Krusienski, D. and Hao, Z.
A Flexible PET-based Wearable Sensor for Arterial Pulse Waveform Measurement.
DOI: 10.5220/0005698000660075
In *Proceedings of the 9th International Joint Conference on Biomedical Engineering Systems and Technologies (BIOSTEC 2016) - Volume 1: BIODEVICES*, pages 66-75
ISBN: 978-989-758-170-0

preserving the attractive features of the sensor array, this paper presents a PET-based sensor for arterial pulse waveform measurement. With a flexible substrate, this sensor bears the same design of a Pyrex-based sensor previously developed by our group (Cheng et al., 2013; Gu et al., 2013). The core of the sensor is a single polydimethylsiloxane (PDMS) microstructure embedded with an electrolyte-enabled resistive transducer array underneath. The spatial resolution of 1.5mm of the transducer array allows aligning one of them right at the site of an artery with a negligible margin. A simple, low-cost fabrication process is developed for realizing this PET-based sensor, where a new bonding process is employed to strengthen the bonding between the PDMS microstructure and the PET substrate with indium titanium oxide (ITO) electrodes. The fabricated sensor is further utilized to measure carotid arterial pulse waveforms of three subjects and radial arterial pulse waveforms of one subject, and the measured results are compared with the related information in the literature for demonstrating its feasibility.

2 SENSOR DESIGN AND FABRICATION

2.1 Sensor Design

Figure 1 depicts the configuration of the PET-based sensor. The sensor encompasses a rectangular PDMS microstructure embedded with an electrolyte-filled microchannel, and a set of ITO electrode pairs distributed along the microchannel length. The portion of electrolyte across an electrode pair functions as a resistive transducer, whose resistance varies with the bottom deflection of the microstructure at its location and is routed out by the electrode pair. Thus, together with the set of electrode pairs, one body of electrolyte in the microchannel forms a 5×1 transducer array with a spatial resolution of 1.5mm.

Distributed deflection acting on the top of the microstructure translates to the bottom deflection of the microstructure and thus geometrical changes of the microchannel, which register as resistance changes by the transducer array. Table 1 summarizes the key design parameters of the sensor. The details of the sensor design can be found in the literature (Cheng et al., 2013; Gu et al., 2013).

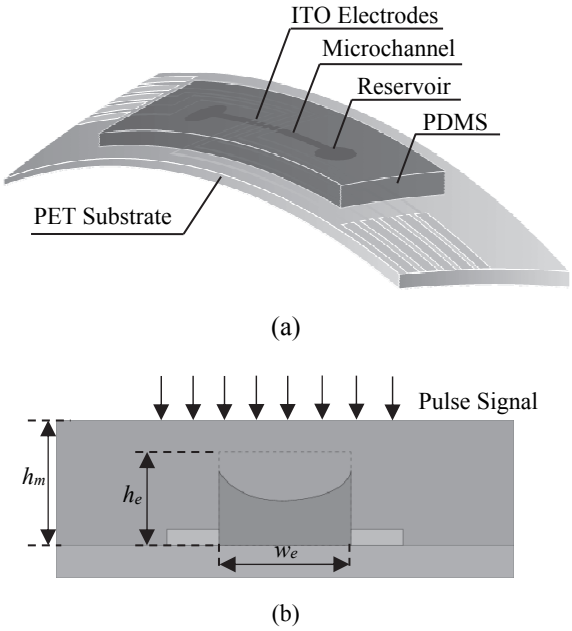

Figure 1: Configuration of microfluidic sensor: (a) 3D view with labelling; (b) side view with key design parameters being labelled.

Table 1: Key design parameters of the PET-based sensor.

Parameter	Value	Symbol
Microchannel cross-section	$1mm \times 80\mu m$	$w_e \times h_e$
Microchannel length	$30mm$	L_e
Spatial resolution	$1.5mm$	d_e
Microstructure thickness	$1.2mm$	h_m

2.2 Fabrication Process

Figure 2 illustrates a low-cost, two-mask fabrication process for realizing the PET-based sensor. The process starts with a commercial ITO/PET sheet (a 0.2mm-thick PET substrate coated with 120nm~160nm-thick ITO layer). To pattern ITO electrodes on the PET substrate, a 15μm-thick dry film (Alpho NIT 215, NichigoMorton Co., Ltd.) is laminated onto the PET substrate. Via the first mask, electrode pattern is transferred to the dry film, which is followed by wet etching of the ITO layer to form ITO electrodes. Afterward, the dry film is removed using ethanol. Via the second mask, a SU8 mold is created on a Pyrex substrate. Then, a mixture of curing agent to PDMS elastomer with a weight ratio of 1:10 is poured over the SU8 mold. After being cured at room temperature over 24hrs, the microstructure is peeled off from the SU8 mold and a hole is punched into each reservoir using a needle.

To strengthen the bonding strength between the PDMS microstructure and the PET substrate with

patterned ITO electrodes, a chemical gluing strategy is adopted (Tang and Lee, 2010, Tsuwaki et al., 2014). First, photoresist is placed onto the microchannel of the microstructure. Then, the patterned ITO electrodes and the microstructure are activated with hydroxyl groups by an oxygen plasma treatment for 1 minute, which are followed by immersing the microstructure and ITO electrodes into 1% (v/v) 3-Glycidyloxypropyltrimethoxysilane (GOPTS) and 5% (v/v) 3-Aminopropyltriethoxysilane (APTES) for 20 minutes, respectively. Afterward, the microstructure is rinsed with acetone, isopropanol and DI water, and, sequentially, the PET substrate with patterned ITO electrodes is rinsed with ethanol and DI water. Finally, the microstructure and the PET substrate are aligned and bonded under a contact pressure at 100 ℃ for 5 minutes, then at 50 ℃ for 24hrs. Electrolyte, 1-ethyl-3-methylimidazolium tricyanomethanide (EMIM TCM), is injected into the microchannel via a reservoir using a syringe. Two reservoirs are then sealed with PDMS with a weight ratio of 1:10. Conductive epoxy is used to make electrical connection between the contact pads of the sensor and the associated electronics on PCBs. Figure 2 shows a couple of pictures of the fabricated PET-based sensor.

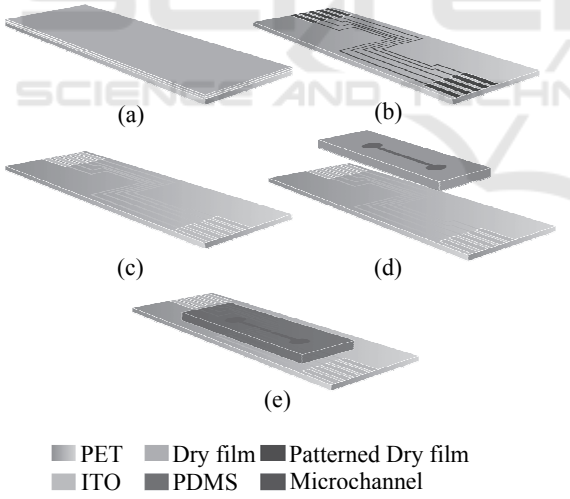

Figure 2: Fabrication process for the PET-based sensor. (a) Dry film lamination. (b) Patterning of dry film. (c) Patterned ITO electrodes. (d) Alignment and bonding with microstructure. (e) 3D view of the sensor.

3 ARTERIAL PULSE WAVEFORM MEASUREMENT AND SIGNAL PROCESSING

The measurements of arterial pulse waveform are conducted on three subjects (a 16yr-old female teenager, a 28yr-old female adult and a 28yr-old male adult) in a quiet environment, after resting for several minutes and no drinking and eating for over 1hr. All the pulse signals are taken from the carotid artery at the right of the neck, except one is taken from a radial artery. Additionally, two subjects are required to do 5min-long strenuous exercise and their carotid pulse signals are taken immediately after exercise from the same location as at rest.

3.1 Pulse Waveform Measurement

As shown in Figure 3(c), the PET-based sensor is placed at the site of the carotid artery and is pressed against it with two fingers. Note that the hold-down pressure against an artery is uncontrollable. The arterial pulse exerts a time-varying deflection on the top of the PDMS microstructure, which registers as a resistance change by the transducer at the site of the artery.

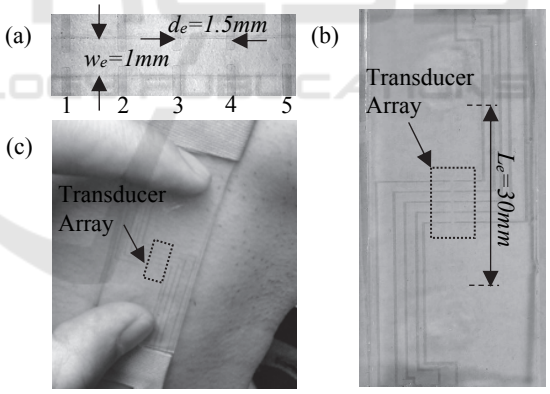

Figure 3: Pictures of the fabricated PET-based sensor. (a) The transducer array with labelling. (b) The whole sensor. (c) Demonstration of how the sensor is held for carotid arterial pulse waveform measurement: two fingers holding the sensor above the carotid artery.

To monitor resistance changes in the transducer array, a function generator is used to apply an Alternating Current (AC) signal (100kHz, peak-peak amplitude: 220mv) as the input signal for all the transducers (Cheng et al., 2013). The output of a transducer is connected to its electronics implemented on PCB for both amplifying the AC signal coming out from the transducer and

converting the AC signal to a Direct Current (DC) output, which is recorded by a LabVIEW program. Note that the same design of electronics is used for all the transducers, but is implemented on separate PCBs. The circuit design can be found in our previous work (Gu et al., 2013). Each pulse is recorded for a 10s period. The sampling rate is kept at 500Hz. Later on, 25 data points per second are utilized for the extracted pulse waveform from an originally recorded pulse signal.

3.2 Signal Processing for Converting Resistance Changes to Pulse Waveforms

As mentioned above, the recorded parameter of a transducer is a DC voltage output, V_{out}, which is related to the resistance of a transducer by (Cheng et al., 2013; Gu et al., 2013):

$$V_{\text{out}} = \frac{v_{pp}^2 R_F^2}{8R^2} \tag{1}$$

where v_{pp} is the peak-to-peak value of the AC signal, and R_F is the feedback resistance of the electronics used. Therefore, the resistance of a transducer can be obtained by:

$$R = \frac{v_{pp} R_F}{2\sqrt{2V_{out}}} \tag{2}$$

The bottom deflection at a transducer is represented by the resistance change:

$$\Delta R = \frac{v_{pp} R_F}{2\sqrt{2}} \left(\frac{1}{\sqrt{V_{out}}} - \frac{1}{\sqrt{V_{out0}}} \right) \tag{3}$$

where V_{out0} is the DC voltage of a transducer, when it is free of deflection.

Owing to fabrication variation in transducer height, h_e, (the smallest design parameter), the original resistance (defined as the resistance of a transducer when it is free of deflection) may vary among the transducers. The original resistance of the i^{th} transducer is roughly calculated as (Yang et al., 2015):

$$R_{0\text{-}i} = \frac{\rho \cdot w_e}{d_e / 2 \cdot h_{e-i}} \tag{4}$$

where ρ is the electrical conductivity of EMIM TCM, d_e, w_e and $h_{e\text{-}i}$ are the length, width and height of the i^{th} transducer, respectively. We further define the resistance of a transducer after being pressed against an artery as its initial resistance, $R_{0\text{-}i}'$. As such, the resistance change is calculated relative to the initial resistance, instead of the original resistance:

$$\begin{aligned} \Delta R &= R_i - R_{0-i}' \\ &= \frac{\rho \cdot w_e}{d_e / 2 \cdot h_{e-i}'} \cdot \left[\left(1 - \frac{z_{s-i}}{h_{e-i}'} \right)^{-1} - 1 \right] \\ &= \frac{\rho \cdot w_e}{d_e / 2 \cdot (h_{e-i}')^2} \cdot z_{s-i} = \frac{(R_{0-i}')^2 \cdot d_e / 2}{\rho \cdot w_e} \cdot z_{s-i} \end{aligned} \tag{5}$$

where $z_{s\text{-}i}$ is the deflection for the i^{th} transducer, $h_{e\text{-}i}$ is the initial height of the transducer.

Since the hold-down pressure against an artery is not controllable, the initial resistances of the sensor vary among all the measurements. According to Equation (5), the sensor deflection at the i^{th} transducer can be obtained:

$$z_{s-i} = \frac{\Delta R}{(R_{0-i}')^2} \cdot \frac{\rho \cdot w_e}{d_e / 2} \tag{6}$$

3.3 Signal Processing for Baseline Drift Removal

The respiration and motion artifact (i.e., motion of the sensor and the body during measurement) can introduce baseline drift to the recorded pulse waveform. The Discrete Meyer Wavelet Transformation (DMWT) and Cubic Spline Estimation (CSE) have been implemented for removing baseline drift from the recorded data (Xu et al., 2007). DMWT is well known for representing localized variations in a signal simultaneously in the time and frequency domains. CSE is used to detect the amplitude envelope of the signal.

Because the baseline drift introduced by respiration and the body and sensor's motion has nonlinear and quasi-periodic contents, linear interpolation estimation has been proven ineffective (Xu et al., 2007). In contrast, a high-degree polynomial is smooth, but it may cause the Runge phenomenon, which increases the error of the signal (Xu et al., 2007). Thus, CSE is widely used and is adopted in this work to remove the baseline drift when the Energy Ratio (ER) of the recorded data reaches a threshold.

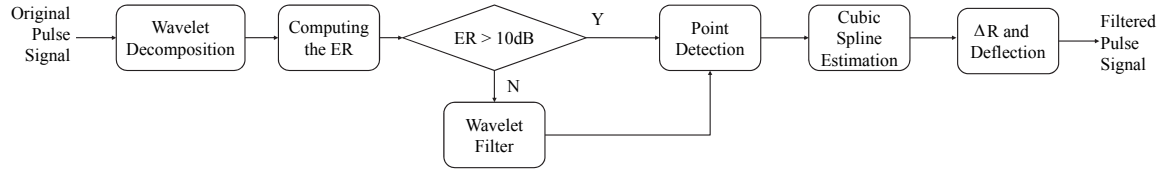

Figure 4: Flow chart of signal processing for pulse waveforms (Xu et al., 2007).

In DMWT, a function is defined in frequency domain:

$$\psi(\mathrm{w}) = \begin{cases} (2\pi)^{-1/2} \times e^{jw/2} \times \sin\left(\frac{\pi}{2} \times v\left(\frac{3}{2\pi}|w|-1\right)\right) \\ \qquad , \frac{2\pi}{3} \le |w| \le \frac{4\pi}{3} \\ (2\pi)^{-1/2} \times e^{jw/2} \times \cos\left(\frac{\pi}{2} \times v\left(\frac{3}{4\pi}|w|-1\right)\right) \\ \qquad , \frac{4\pi}{3} \le |w| \le \frac{8\pi}{3} \\ 0 \qquad , |w| \notin \left[\frac{2\pi}{3}, \frac{8\pi}{3}\right] \end{cases} \quad (7)$$

where *v(x)* is an auxiliary function expressed as (Xu et al., 2007):

$$v(x) = x^4(35 - 84x + 70x^2 - 20x^3), x \in [0,1] \quad (8)$$

Figure 4 depicts the flow chart of signal processing for removing the baseline drift from the original pulse signal, while Figure 5 illustrates the corresponding intermediate results of the signal processing. First, we utilize CSE to obtain the baseline envelope of the recorded resistance signal. Figure 5(a) shows both the recorded resistance signal, converted from the DC output voltage signal using Equation (2), and the approximated baseline of the signal via CSE as a function of time.

During the measurement post-exercise, there are three to five respiration cycles for a 10s period. The motion artifacts are the low frequency components. The main frequency of baseline drift is less than 1Hz. The cutoff frequency of the fourth-level scale function is 1.56Hz. And the frequency content of the pulse waveform is less than 40Hz. Thus, (A1−A4) and A4 are used to approximate the pulse signal and its baseline drift, respectively. Thus, we apply DMWT to the resistance signal to obtain its first-level approximation, A1, and its fourth-level approximation, A4, as shown in Figure 5(b). The two approximations are utilized to compute the ER of the recorded pulse signal as below:

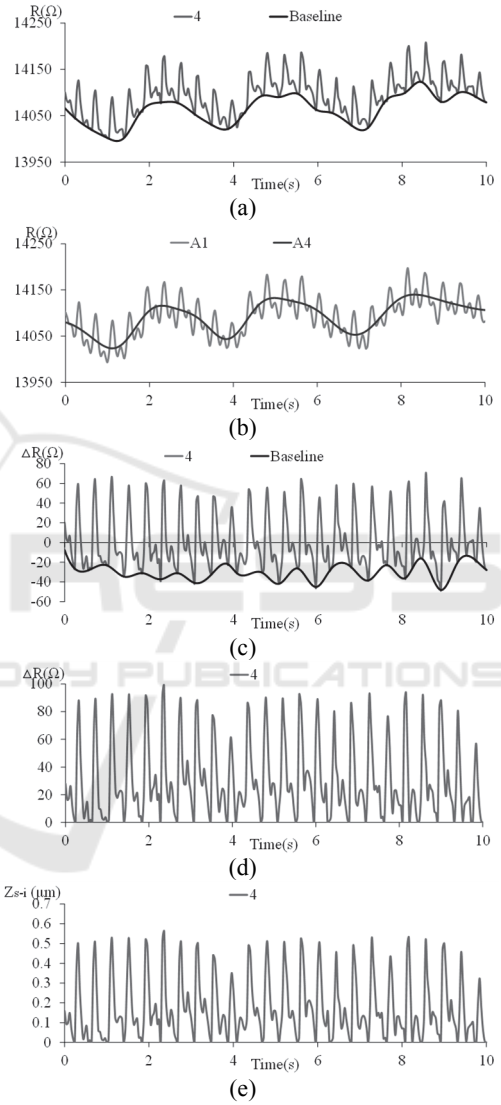

Figure 5: The corresponding intermediate results of the signal processing using DMWT and CSE. (a) Resistance with estimated baseline. (b) The first-level and fourth-level approximation content of pulse decomposition. (c) The resistance change with estimated baseline. (d) The resistance change. (e) Sensor deflection at the 4th transducer.

$$ER = 20\log_{10}\frac{\|A1 - A4 - mean(A1 - A4)\|}{\|A4 - mean(A4)\|} \quad (9)$$

where || || represents the order-two norm, *mean*|| *A1-A4*|| represents the average of *A1-A4*.

ER is used to quantify the extent of the baseline drift. It is found that a pulse signal exhibits little base drift when its ER is higher than 10dB. Therefore, 10dB is selected as the ER threshold for removing the baseline drift from the recorded resistance signal. If ER is higher than 10 dB, the baseline drift is removed by subtracting the approximated baseline in Figure 5(a) from the recorded resistance signal. If ER is lower than 10dB, the baseline drift is removed by subtracting A4 in Figure 5(b) from the recorded resistance signal. Then, we obtain the resistance change of the recorded resistance signal, as shown in Figure 5(c). However, the pulse waveform still contains baseline drift. CSE is used again to obtain the baseline drift of the resistance change, as shown in Figure 5(c). Afterward, the resistance change in Figure 5(c) is subtracted by this new baseline drift to obtain the resistance change in Figure 5(d). Finally, based on Equation (6), the resistance change in Figure 5(d) is converted to the sensor deflection, as shown in Figure 5(e). The sensor deflection captures the pulse waveform without being distorted by the baseline drift. All the pulse signals measured on a subject at rest have an ER value higher than 10dB, while the pulse signals measured on a subject post-exercise have an ER value lower than 10dB.

4 MEASURED RESULTS

Our goal for the sensor in this work is to aquire the pulse waveform of a subject so as to evaluate some physiological parameters related to the cardiovascular system. Certainly, with an oscillometric device (Digiglio et al., 2014), the measured results can be further processed to obtain the absolute values for blood pressure. To demonstrate the feasiblity of the sensor for pulse waveform measurement, carotid arterial pulse waveforms are measured by the sensor on three subjects at rest and on two subjects post-exercise. Additionally, radial arterial waveforms are measured on one subject at rest. Note that since we recently started to explore the sensor for pulse waveform measurement, the data collected here is not comprehensive. Nevertheless, the measured pulse waveforms are compared with the related information in the literature for the feasibility of using the sensor for pulse waveform monitoring.

4.1 Robustness to Motion Artifact

Motion artifact from the respiration and the handshaking during measurement are unavoidable. Sometimes, it is needed to assess arterial pulse waveform difference between before-exercise and post-exercise. As such, the sensor needs to be immune to motion artifact. Figure 6 shows the measured resistances of the five transducers measured on the 16-yr female post-exercise. The 4th and 5th transducers capture not only a clear patterned pulse signal but also the heavily-breathing pattern, indicating that the carotid artery is between the two transducers. The breathing pattern introduces extremely large baseline drift to the recorded pulse signal. However, as will be seen in the next subsection, the sensor is capable of obtaining the undistorted pulse waveform under such severe motion artifact.

The rest three transducers obtain random signals with a respiration pattern, indicating that these transducers are away from the carotid artery. Note that this measurement indicates that the transducers do not interfere with each other. Thus, the sensor provides a negligible alignment margin for a untrained individual to use.

4.2 Carotid Pulse Waveforms at-Rest and Post-Exercise

The same sensor is used to conduct all the pulse measurements on the carotid artery. Thus, variation in pulse waveform among the three subjects arises mostly from their cardiovascular system conditions, in the sense that hold-down pressure may affect the pulse waveform slightly, according to Equation (6). Quantification of the effect of hold-down pressure on the measured pulse waveform needs to be further studied in the future. The measurement on the carotid artery of each subject was repeated several times. For each measurement, pulse signal typically shows up in two or three transducers. For consistence, we simply choose the pulse signal from the 4th transducer for comparison. Thus, the sensor deflection at this transducer is used to present a measured pulse waveform.

Figure 7(a) compares the pulse waveforms measured on the three subjects at rest and Figure 7(b) compares the pulse waveforms measured on onsets of the first pulses of the subjects are set at the same

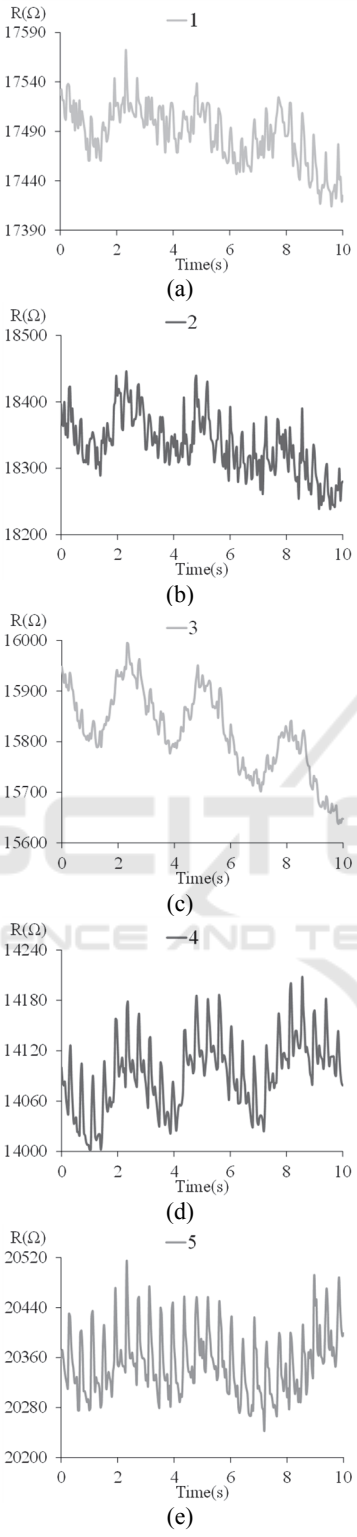

Figure 6: Arterial waveform patterns of five transducers from the 16yr-old female teenager post-exercise. (a)-(e) are recorded resistance of each transducer.

time instant. While the hold-down pressure against a carotid artery is larger at-rest than post-exercise, the sensor deflection is larger at rest than post-exercise, as can be seen in Figure 7. This indicates that a strong pulse from post-exercise does not directly translate to a large sensor deflection, without a large hold-down pressure.

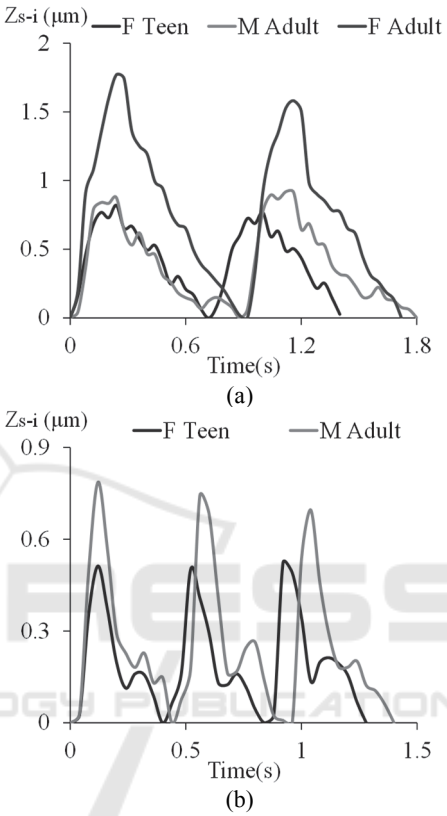

Figure 7: Carotid pulse waveform in terms of the sensor deflection at the 4th transducer at-rest (a) and post-exercise (b).

Figure 8(a) shows the aorta pressure waveform in the comparison between two adults: a 68-year old individual and his 37-year-old son (O'Rourke and Hashimoto, 2007). The pulse pattern varies with ages. Since carotid artery is central and thus is representative of aorta pressure. Evidently, the pulse waveforms of the 28yr-old male and 16yr-old female (both physically active) at rest exhibit a quite vertical up-stroke and are similar to the one of the young man. In constrast, containing an inclined up-stroke, the pulse waveform of the 28yr-old female (not physically active) at rest is closer to the one of the old man.

The 28yr-old female has the lowest pulse rate but the highest pulse strength. This high pulse strength might be due to the artery being close to the skin.

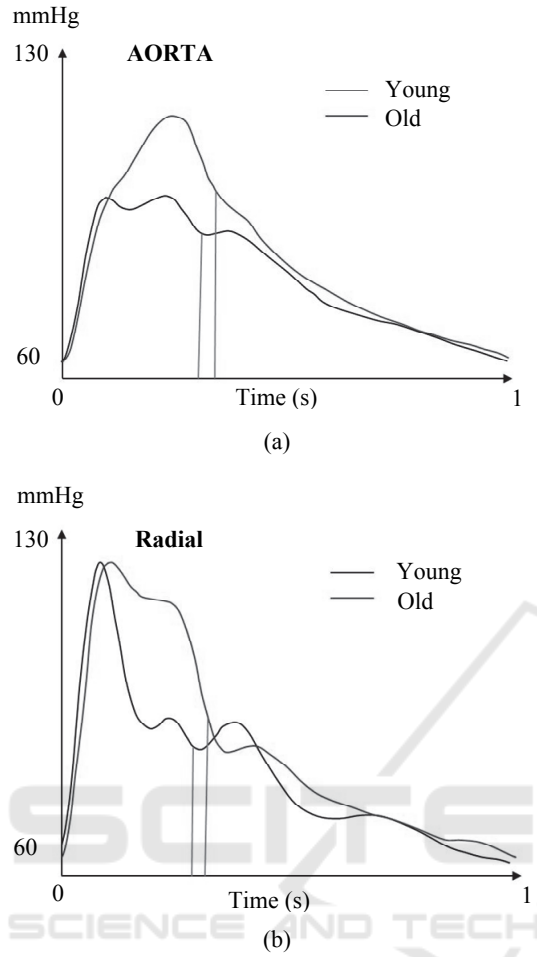

Figure 8: Aortic (a) and radial (b) pressure wave in 36-year-old man (young) and his 68-year-old father (old) (O'Rourke and Hashimoto, 2007).

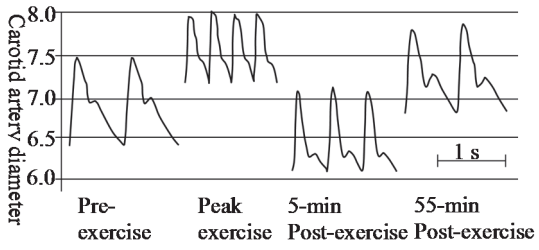

Figure 9: Carotid artery distension wave and blood pressure recordings before, during and after dynamic exercise. Carotid artery distension wave recordings and corresponding blood pressure values in one representative subject during the control period, at peak-exercise, and at 5 and 55 min post-exercise. Time scale = 1s. (Studinger et al., 2003, with permission).

The 16yr-old female has a faster pulse rate than the 28yr-old male both at rest and post-exercise. The dicrotic notch in the pulse waveforms of the two subjects post-exercise is much lower than its counterpart at rest. Figure 9 shows a similar difference in pulse waveform between at rest (control) and post-exercise. Thus, our measurement (Figure 7) is consistent with that in the literature.

4.3 Radial Arterial Pulse Waveforms

Another PET-based sensor is used to measure the radial pulse of the 28yr-old female, with the sensor being aligned in parallel with and perpendicular to the radial artery. Figure 10 illustrates the measured pulse waveforms under the two alignments. In the parallel alignment, three transducers, 1, 2 and 3, are at the site of the artery, while only transducer 3 is at the site of the artery in the perpendicular alignment.

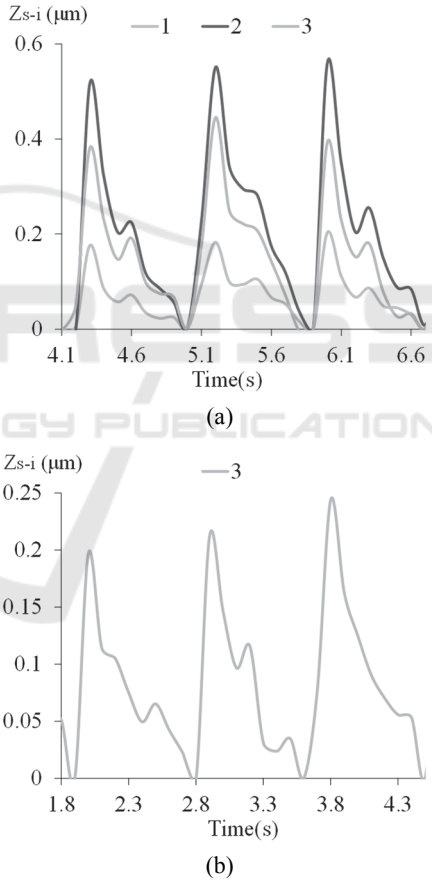

Figure 10: The radial artery pulse measurement for 28yr-old female adult. (a) The sensor aligned parallel with the radial artery. (b) The sensor aligned perpendicular to the radial artery.

The pulse waveform varies between the two alignments, which is believed to result from the sensor being more loosely in contact with the artery in the perpendicular alignment than in the parallel

alignment. Thus, the pulse waveform in Figure 10(a) is believed to be correct and is compared with the one in Figure 8(b), showing a little bit away from the one of the young man.

4.4 Arterial Tonometric Parameters

Figure 11 illustrates a typical cycle of a measured pulse signal, which includes main arterial tonometric parameters often used to characterize the waveform (Velik, 2015). The physical meaning of the tonometric parameters in the figure is given in Table 2.

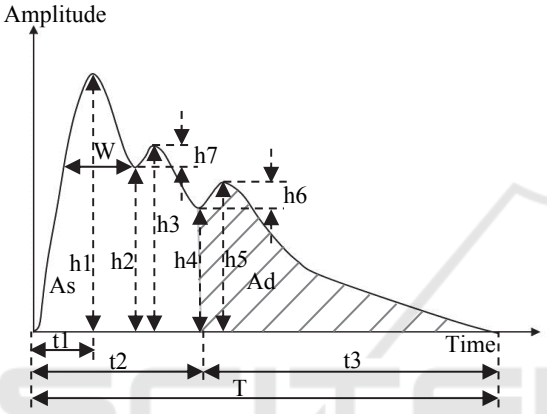

Figure 11: Parameters of pulse wave signal (Velik, 2015).

According to Figure 11, the arterial tonometric parameters of the subjects are calculated and summarized into Table 2. The ratio of h1/h5 is calculated, instead of the absolute values of h1 and h5, due to the lack of a device for calibration. The radial pulse measurement under the parallel alignment is included in the table. As mentioned previously, the ratio of h1/h5 post-exercise is higher than at rest, which is observed on the 16yr-old female and the 28yr-old male. It has been found that as the pulse transmits from central (carotid) to peripheral (radial), the ratio of h1/h5 goes up (McEniery et al., 2014) and the up-stroke time (t1) becomes shorter (Hurst, 1982). The measured results on the 28yr-old female are in good agreement with these findings. Note that two different sensors of the same design are used to measure the carotid and radial arterial pulse waveforms of the 28yr-old female. The consistency of the results on the carotid artery and the radial artery (the ratio of h1/h5 going up and the up-stroke time being shorter from carotid to radial) simply prove the robustness of the sensor.

We envision that this flexible sensor can be attached on a bracelet and can then be worn on the wrist loosely, together with integrated circuit for signal routing and wireless transmission. Whenever an individual needs to measure the radial pulse waveform, he can align the sensor at the site of the artery and press the sensor against the artery with his fingers. To measure the carotid artery, the bracelet can be taken off the wrist and put the sensor on the neck. Owing to the small size and flexibility of the sensor, it is expected to be comfortable to wear a bracelet with the sensor.

Table 2: Measured arterial tonometric characteristics from the subjects.

Variables	Description	Carotid artery					Radial artery
		Female Teenager		Male Adult		Female Adult	Female Adult (parallel)
		At-rest	Post-exercise	At-rest	Post-exercise	At-rest	At-rest
h1/h5	Amplitude of main peak / Amplitude of dicrotic wave	1.551	3.202	1.415	3.251	1.876	2.296
t1(s)	Duration between onset and peak point	0.24	0.12	0.24	0.12	0.24	0.1
t2(s)	Duration between onset and incisura	0.4	0.24	0.32	0.28	0.36	0.3
t3(s)	Duration between onset and dicrotic	0.32	0.16	0.56	0.16	0.52	0.5
T(s)	Time in one pulse cycle	0.72	0.4	0.88	0.44	0.88	0.8

5 CONCLUSION

This paper presents a PET-based wearable sensor for arterial pulse waveform measurement for untrained individuals to conduct the arterial pulse waveform measurement. The sensor contains a PDMS microstructure embedded with a 5×1 resistive transducer array, spanning 6mm and with a spatial resolution of 1.5mm. Built on PET substrate, the sensor is fabricated using a low-cost, two-mask fabrication process. To demonstrate its feasibility for arterial pulse waveform measurement, one sensor is used to measure carotid arterial pulse waveform of three subjects at rest and two subjects post-exercise, while another sensor of the same design is used to measure radial arterial pulse waveform of one subject at rest. The respiration and motion artifact introduces baseline drift to originally recorded pulse signal. A combination of DMWT and CSE is utilized to effectively remove the baseline drift in a pulse signal. The robustness of the sensor to baseline drift is demonstrated by the pulse signals measured on a subject post-exercise. After its baseline drift being removed, an arterial pulse waveform is expressed in terms of the sensor deflection as a function of time. All the measured pulse waveforms of carotid and radial arteries of the three subjects at rest and post-exercise are consistent with their counterparts in the literature, thus demonstrating the feasibility of using the sensor as a wearable health monitoring device.

REFERENCES

Cheng, P., Gu, W., Shen, J., Ghosh, A., Beskok, A. and Hao, Z., 2013. Performance study of a PDMS-based microfluidic device for the detection of continuous distributed static and dynamic loads. *Journal of Micromechanics and Microengineering,* 23(8), p. 085007.

Digiglio, P., Li, R., Wang, W. and Pan, T., 2014. Microflotronic arterial tonometry for continuous wearable non-invasive hemodynamic monitoring. *Annals of biomedical engineering,* 42(11), pp.2278-2288.

Gu, W., Cheng, P., Ghosh, A., Liao, Y., Liao, B., Beskok, A. and Hao, Z., 2013. Detection of distributed static and dynamic loads with electrolyte-enabled distributed transducers in a polymer-based microfluidic device. *Journal of Micromechanics and Microengineering,* 23(3), p.035015.

Hu, C. S., Chung, Y. F., Yeh, C. C., and Luo, C. H., 2011. Temporal and spatial properties of arterial pulsation measurement using pressure sensor array. *Evidence-Based Complementary and Alternative Medicine, 2012*.

Hurst, J. W. and Logue, R. B., 1982. *The heart: arteries and veins*, McGraw -Hill, pp.170-179.

Lin, W. H., Zhang, H. and Zhang, Y. T., 2013. Investigation on cardiovascular risk prediction using physiological parameters. *Computational and mathematical methods in medicine, 2013*.

McEniery, C. M., Cockcroft, J. R., Roman, M. J., Franklin, S. S. and Wilkinson, I. B., 2014. Central blood pressure: current evidence and clinical importance. *European heart journal,* 35(26), pp.1719-1725.

O'Rourke, M. F. and Hashimoto, J., 2007. Mechanical factors in arterial aging: a clinical perspective. *Journal of the American College of Cardiology,* 50(1), pp.1-13.

Saugel, B., Fassio, F., Hapfelmeier, A., Meidert, A. S., Schmid, R. M., and Huber, W., 2012. The T-Line TL-200 system for continuous non-invasive blood pressure measurement in medical intensive care unit patients. *Intensive care medicine*. 38(9), pp.1471-1477.

Studinger, P., Lenard, Z., Kovats, Z., Kocsis, L. and Kollai, M., 2003. Static and dynamic changes in carotid artery diameter in humans during and after strenuous exercise. *The Journal of physiology,* 550(2), pp.575-583.

Tang, L. and Lee, N. Y., 2010. A facile route for irreversible bonding of plastic-PDMS hybrid microdevices at room temperature. *Lab on a Chip,* 10(10), pp.1274-1280.

Tsuwaki, M., Kasahara, T., Edura, T., Matsunami, S., Oshima, J., Shoji, S., Adachi, C. and Mizuno, J., 2014. Fabrication and characterization of large-area flexible microfluidic organic light-emitting diode with liquid organic semiconductor. *Sensors and Actuators A: Physical,* 216, pp.231-236.

Velik, R., 2015. An objective review of the technological developments for radial pulse diagnosis in Traditional Chinese Medicine. *European Journal of Integrative Medicine,* 7(4), pp.321-331.

Xu, L., Zhang, D., Wang, K., Li, N. and Wang, X., 2007. Baseline wander correction in pulse waveforms using wavelet-based cascaded adaptive filter. *Computers in Biology and Medicine,* 37(5), pp. 716-731.

Yang, Y., Shen, J. and Hao, Z., 2015. A two-demensional (2D) distributed deflection sensor for tissue palpation with correction mechanism for its performance variation. *under review*.